Precise Vehicle Localization Using Multiple Sensors and Natural Landmarks

Ullrich Scheunert
Chemnitz University
of Technology (CUT),
Reichenhainer Strasse 70
09126 Chemnitz
Germany
scheunert@infotech.
tu-chemnitz.de

Heiko Cramer
Chemnitz University
of Technology (CUT),
Reichenhainer Strasse 70
09126 Chemnitz
Germany
cramer@infotech.
tu-chemnitz.de

Gerd Wanielik
Chemnitz University
of Technology (CUT),
Reichenhainer Strasse 70
09126 Chemnitz
Germany
wanielik@infotech.
tu-chemnitz.de

Abstract - *Localization of automobiles in road environments is an important task in the field of developing driver assistance systems, focussing on the improvement of safety and comfort. It is not only essential for navigation systems but offers the possibility to create reliable and precise warning systems and vehicle control functions.*
Besides the internal odometric sensors, especially the GPS and DGPS are standard sensors for localization. But the DGPS is not sufficient for localization in adverse – especially urban – areas, because the satellite information is often not available. This is the reason why a system for an urban environment is presented that uses additionally absolute position measurements based on natural landmarks. A Kalman filter fuses the standard odometric measurements and DGPS with measurements of landmarks in the form of a point or a line, which are detected in video images and laser scanner measurements. So the system reaches high precision for vehicle localization.

Keywords: localization, sensor data fusion, Kalman filter, tracking, landmarks, urban traffic.

1 Introduction

Research from recent years has shown that previous knowledge is needed urgently to develop highly reliable advanced driver assistance systems. The importance of calculating a precise self localization is obvious, because previous knowledge about the spatial environment or about spatiotemporal events provided by geographic information systems can only be used if a precise self localization is available, too.

The need for precise localization is especially apparent in environments where the density of obstacles is high and the pre-given vehicle paths are very precise, too. This is the case in urban environments where there are a lot of cars and pedestrians and other moving and standing obstacles. Contrary to most of the applications working today in navigation systems, not only the lateral position is needed in urban environments but also the longitudinal position. Only in this way it can be avoided, that the vehicle runs outside the pre-given lane, misses crossroads or goes onto the pavements, causing fatal attacks on pedestrians.

However the localization knowledge will not only help to build up more precise navigation systems for urban environments, but will also support surveillance systems for cars, that have the task of detecting and tracking the paths of vehicles and pedestrians in the observed environment.

The standard sensor used presently for localization is the GPS or DGPS. But especially in urban environments, principle based errors can occur, e.g. abrupt changes in the GPS position readings caused by a sudden obstruction of the line of sight access to satellites or multi-path effects, as well as gradual changes caused by changes in atmospheric conditions.

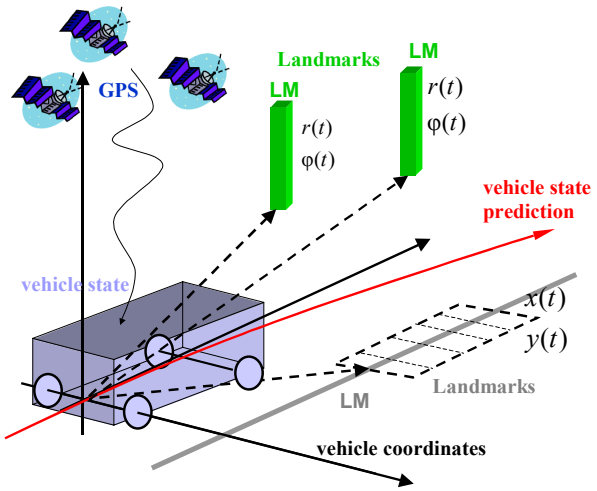

Fig. 1. Vehicle localization scenario using landmarks.

Therefore, we propose an approach and a system that would use additional measurements to the information from GPS and odometric sensors of the vehicle. These would consist of the knowledge of a map (GIS) of the urban environment with the special information about

landmarks inside the map (see figure 1), and also sensors capable of detecting these landmarks.

As a test platform for the localization an electro mobile car is used that is equipped with all necessary sensors like DGPS and odometric sensors (see figure 2) as well as sensors for the detection of landmarks in the form of a point (point-style) or a line (line-style).

Nr.	Sensoren
1	Velocity measurement
2	compass
3	Angular velocity
4	GPS (DGPS)
5	CCD Camera
6	Laser Scanner

Fig. 2. Electro mobile test car.

For the test environment, an urban area is chosen at the campus region of Chemnitz University of Technology (CUT) where situations like street crossings and turnings occur and where problems in the GPS reception are well known (see figure 3).

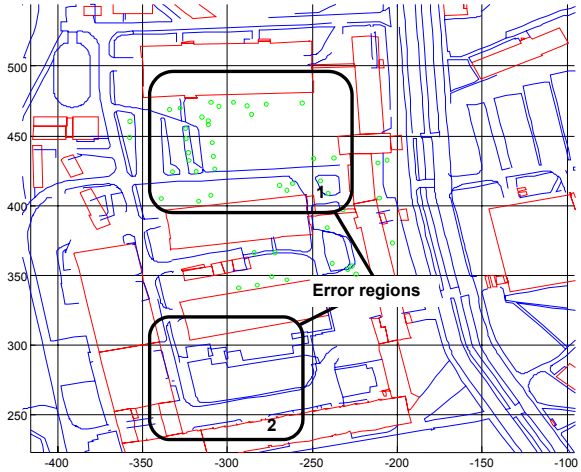

Fig. 3. Test regions selected with known problems in GPS reception.

The paper describes the main steps necessary for building up a Kalman filter based multi sensor data fusion system for localization in urban environments, supported by the use of natural landmarks. The following section, section 2, deals with the first task of choosing a suitable movement model for the vehicle. Section 3 gives an overview over the sensor models which are used together with the odometric movement sensors of the car. Section 4 introduces the use of the landmarks for the localization and the nonlinear sensor models in this case. Section 5 gives a summary and a concluding presentation of the results.

2 Movement Model for the Vehicle

Choosing a suitable movement model is very important in the creation process of the Kalman filter as it does not only define the set of state variables but also determines in which way the movement has constraints over time and where uncertainties occur in the modelling. Some criteria are discussed that allow selecting the best suited model. As using only the best model seems to be more evident than using a couple of models in a multiple model system, one model is selected in this section which is rated best. Three models will be taken into account under this point of view.

2.1 Constant Acceleration Model

The most direct and simplest movement model for vehicles is the constant acceleration model ([1], [2]) that assumes that the vehicle behaves like a mass and stays with a constant acceleration in both directions ${}^{w}x(t)$ and ${}^{w}y(t)$ where the upper left index denotes that it is a variable in the world coordinate system. The movement behaviour is assumed to be decoupled in these two directions. Small changes in the movement state are thought to be caused by disturbances in the acceleration components ${}^{w}\ddot{x}(t)$ and ${}^{w}\ddot{y}(t)$. The according state space vector is shown below.

$$ {}^{w}\underline{x}_{ca/v}(t) = \begin{bmatrix} {}^{w}x(t) \\ {}^{w}\dot{x}(t) \\ {}^{w}\ddot{x}(t) \\ {}^{w}y(t) \\ {}^{w}\dot{y}(t) \\ {}^{w}\ddot{y}(t) \end{bmatrix} \qquad (1) $$

As this model is linear in the dynamic system equation it has the advantage of more compact Kalman Filter equations.

$$ \frac{d\ {}^{w}\underline{x}_{ca/v}(t)}{dt} = A_{ca}(t)\,{}^{w}\underline{x}_{ca/v}(t) + {}^{w}\underline{v}_{ca/v}(t) \qquad (2) $$

Nevertheless, it has the disadvantage that the variety of possible movement curves is not reduced by means of the kinematic conditions given for a wheeled vehicle.

In addition, the state space does not explicitly contain the heading of the object – in this case the vehicle. If the velocities become occasionally zero, every information about the heading and the expected future movement direction is lost.

2.2 Constant Turn Rate Model

From aeronautic and several automobile applications ([2], [4]) the usage of the constant turn rate model is known where the kinematic conditions given for a wheeled car are respected. As these conditions determine in most cases the movement at a circle, the radius of this circle is taken into account in the state space vector with the help of the angular velocity $\dot{\gamma}(t_k)$ and then we use

$$ {}^{w}\underline{x}_{ctr/v}(t) = \begin{bmatrix} {}^{w}x(t) \\ {}^{w}\dot{x}(t) \\ {}^{w}y(t) \\ {}^{w}\dot{y}(t) \\ {}^{w}\dot{\gamma}(t) \end{bmatrix} \tag{3} $$

as state vector of the constant turn rate model. The dynamic system equation becomes nonlinear in this case

$$ \frac{d\ {}^{w}\underline{x}_{ctr/v}(t)}{dt} = g_{Actr}\left({}^{w}\underline{x}_{ctr/v}(t), t\right) + {}^{w}\underline{v}_{ctr/v}(t) . \tag{4} $$

The heading information however, is also in this model only available when the vehicle is in movement, so when it is stationary or only just started, there is an absence of heading information. As this problem is not solved with the common constant turn rate model, a model containing two enhancements is proposed below.

2.3 Constant Turn Rate Model with Constant Velocity and Heading

To eliminate the disadvantages mentioned above, the position information in the state vector is completed by the heading angle ${}^{w}\gamma(t)$ [5], [7] (the heading angle can be interpreted as the angle at which the vehicle is facing). The velocity of the movement direction – represented before in the two components ${}^{w}\dot{x}(t)$ and ${}^{w}\dot{y}(t)$ – is now substituted by the longitudinal velocity ${}^{w}v(t)$

$$ {}^{w}\underline{x}_{ctrv/v}(t) = \begin{bmatrix} {}^{w}x(t) \\ {}^{w}y(t) \\ {}^{w}\gamma(t) \\ {}^{w}v(t) \\ {}^{w}\dot{\gamma}(t) \end{bmatrix} . \tag{5} $$

The dynamic system equation is also nonlinear in this case

$$ \frac{d\ {}^{w}\underline{x}_{ctrv/v}(t)}{dt} = g_{Actrv}\left({}^{w}\underline{x}_{ctrv/v}(t), t\right) + {}^{w}\underline{v}_{ctrv/v}(t) \tag{6} $$

with

$$ g_{Actrv}\left({}^{w}\underline{x}_{ctrv/v}(t), t\right) = \begin{bmatrix} {}^{w}v(t)\cos\left({}^{w}\gamma(t)\right) \\ {}^{w}v(t)\sin\left({}^{w}\gamma(t)\right) \\ {}^{w}\dot{\gamma}(t_k) \\ 0 \\ 0 \end{bmatrix} . \tag{7} $$

When looked at from the theoretical point of view, this model is suited best for the task of tracking the vehicle's position. It is assumed that even if the conditions of wheel forces are not modelled, small deviations caused by this model's simplification can be corrected by the estimation procedure.

2.4 Comparison of the Movement Models

The suitability of the considered models has been verified by simulations. For that reason a test Kalman filtering was performed using only disturbed simulated GPS position measurements [13].

For the test, three test tracks where used: a linear track, a curved (sinuous) track and a university test track. The simulations show that more or less all models are able to work in a position estimation filter. Nevertheless, the comparison at the basis of the mean square error and the maximum error still shows some differences.

Linear test track:
All models for the filtering in general bring usable results for that track. The difference between the *ca* and the *ctr* result is small. Obviously, the coupling of both velocity components in the new state variable ${}^{w}\dot{\gamma}(t)$ has no significant effect on the results. Contrary to that, the *ctrv* model reduces the error values significantly (see table 1).

Table 1: Performance of the models at Linear test track.

	Mean square error	Maximum error
No filtering	1.418 m (100%)	3.491 m (100%)
ca	0.986 m (69.5%)	2.924 m (83.4%)
ctr	0.968 m (68.3%)	2.874 m (82.3%)
ctrv	0.824 m (58.1%)	2.239 m (64.1%)

Curved test track:
The results of the curved track show values that are similar to those of the linear track. The *ctr* and *ctrv* models can clearly not show their adequacy in that track because it contains a series of changing curves and not a long constant turn as it is the assumption for these models.

Table 2: Performance of the models at Curved test track.

	Mean square error	Maximum error
No filtering	1.518 m (100%)	3.498 m (100%)
ca	1.029 m (67.8%)	2.756m (78.8%)
ctr	0.970 m (63.9%)	2.645 m (75.6%)
ctrv	0.876 m (57.7%)	2.548 m (72.8%)

University test track:
This track summarizes the characteristics of the linear and the curvy track. Its results especially show in the mean square error, that filtering on the basis of the *ctrv* model brings the best results in this comparison. On the other hand, the maximum error shows the necessity of more than only the position sensor, because the position measurements alone can lead the estimated course away from the original in extreme situations and cause incorrect results in a short interval of time.

Table 3: Performance of the models at University test track.

	Mean square error	Maximum error
No filtering	2.477 m (100%)	3.679 m (100%)
ca	1.120 m (45.2%)	3.820 m (103.8%)
ctr	1.070 m (43.2%)	3.749 m (101.9%)
ctrv	0.903 m (36.5%)	2.903 m (78.9%)

When observed from the simulation point of view – as well as from the theoretical – the *ctrv* seems to be the model which is best suited for the task. The following table summarises the previous results and completes the rating by some further conditions [14].

Table 4: Performance of the models summary

	ca	*ctr*	*ctrv*
Theoretical adequacy	*	**	***
Low effort of realisation	***	**	**
Quality of estimation with GPS	*	*	**
Compatibility with additional sensors	*	*	***

As the *ctrv* model is obviously the best for the task it is used for the further steps of filtering. Compatibility with other additional sensors is especially considered in the next section.

3 Sensor Models for Multi Sensor Kalman Filtering

As mentioned before, the *ctrv* model is best suited to the combination with a lot of sensors in a position estimation algorithm because of the suitable constitution of the state space vector. The result is that the sensor models considered here are simply the direct mapping of the state space components of the *ctrv* model.
In the case of the GPS measurements, this benefit is also given if the other movement models are used because all these state vectors contain the position components as measurements.

Sensor GPS

$$\underline{y}_1(t_k) = \begin{bmatrix} x_{GPS}(t_k) \\ y_{GPS}(t_k) \end{bmatrix} = \begin{bmatrix} {}^{w}x(t_k) + w_{xGPS}(t_k) \\ {}^{w}y(t_k) + w_{yGPS}(t_k) \end{bmatrix} \quad (8)$$

As sensors measuring additional movement parameters first the odometric sensors for the longitudinal velocity and the angular velocity are taken into account.

Sensor longitudinal and angular velocity

$$\underline{y}_2(t_k) = \left[v(t_k)\right] = \left[{}^{w}v(t_k) + w_v(t_k)\right] \quad (9)$$

$$\underline{y}_3(t_k) = \left[\dot{\gamma}_z(t_k)\right] = \left[{}^{w}\dot{\gamma}(t_k) + w_{\omega z}(t_k)\right] \quad (10)$$

As a further sensor, a compass sensor that can be integrated easily with a simple linear sensor model is used.

Sensor compass

$$\underline{y}_4(t_k) = \left[\gamma_K(t_k)\right] = \left[{}^{w}\gamma(t_k) + w_{\gamma K}(t_k)\right] \quad (11)$$

Figure 4 shows the test track and the simulated GPS measurements for the test of the Kalman filtering. Several configurations of sensors are used. The test is started with the disturbed GPS measurements and every additional sensor is added step by step.

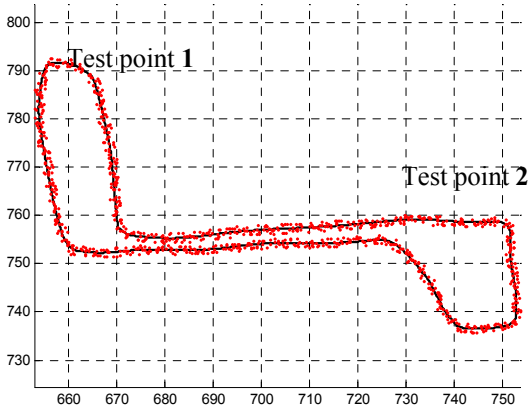

Fig. 4. Simulated test track with simulated noisy GPS signal.

First, the measurements of the angular velocity are added. Next, the measurements of the longitudinal velocity contribute to the estimation and at last the compass is used additionally. The comparison between the results of the different sensor configurations is shown in the four graphs in figure 5 and figure 6.

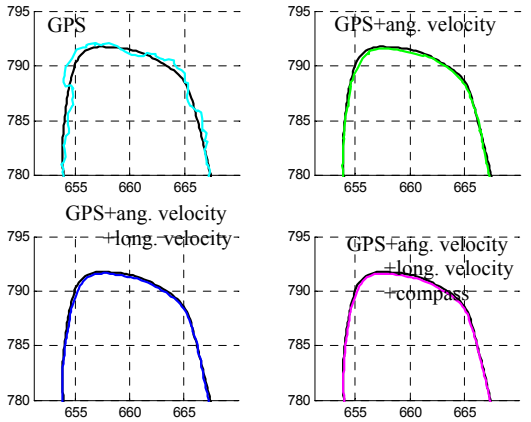

Fig. 5. Estimation results at test point 1 - comparison with the original track.

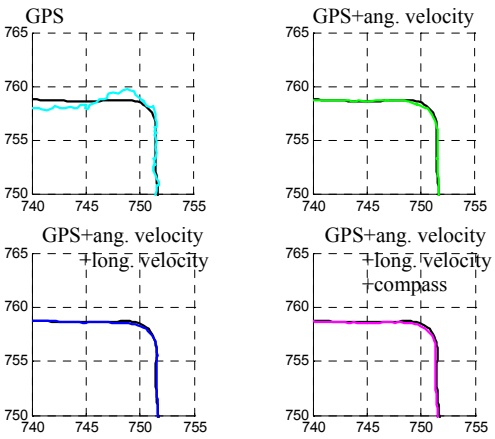

Fig. 6. Estimation result at test point 2 - comparison with the original track.

The results are demonstrated at two test points 1 and 2 with a suitable resolution. It can be seen easily that the first step of adding the angular velocity as the first additional sensor is the most beneficial. The following improvements are smaller but nevertheless can be recognized in the graphs.

Table 5: Performance of the *ctγv* models at University test track with several sensor combinations.

	Mean square error	Maximum error
GPS	0.903 m (100.0 %)	2.913 m (100.0 %)
GPS + angular velocity	0.398 m (44.1 %)	0.972 m (33.4 %)
GPS + angular velocity + long. velocity	0.291 m (32.2 %)	0,504 m (17.3 %)
GPS + angular velocity + long. velocity + compass	0.278 m (30.1 %)	0.479 m (16.4 %)

More obvious is the benefit listed in table 5. Both steps of adding the angular velocity measurements, as well as adding the longitudinal velocity measurements (see the performance of the measurements in table 6) bring significant reductions to the mean and maximum square errors of the estimation result.

Table 6: Performance of the sensors.

	Standard deviation	maximum error
GPS	0.578 m	1.000 m
angular velocity	0.003 rad/s	0.005 rad/s
longitudinal velocity	0.058 m/s	0.100 m/s
compass	0.029 rad	0.050 rad

4 Sensor Models for Landmark Detecting Sensors

Even if the results of table 5 verify the usage of the mentioned sensors, the error values received can not be satisfying. Especially the maximum error is not good enough for urban environments. Also, if the quality of the GPS signal is worse than assumed in the simulations above, further supporting measurement mechanisms are needed as they are provided by using landmarks (see figure 7).

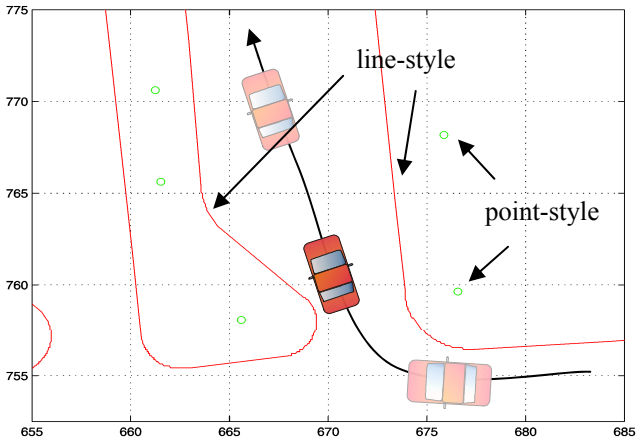

Fig. 7. Simulated movement of the vehicle inside a GIS map containing landmarks.

For this task high precise GIS map material is used in which the shape of the urban roads and its road borders (line-style landmarks) as well as trees and streetlamps (point-style landmarks) are to be found.

For both types of landmarks a two step transformation has to be performed. At first the landmarks ${}^{w}\underline{x}_{lm0}(t_k)$ given in the world coordinate map must be transformed into the local moving coordinate system of the vehicle (see equation (13)). Secondly the "normal" transformation from the vehicle coordinate system to the according sensor measurement space (see equation (14)) is necessary.

These two steps can not be integrated into the original Kalman filter fusion step [1], [11], [12] because the landmarks in the map come attached with their own uncertainties (see equation (12)).

$$ {}^{w}\underline{x}_{lm}(t_k) = {}^{w}\underline{x}_{lm0}(t_k) + {}^{w}\underline{v}_{lm}(t_k) \tag{12} $$

$$ {}^{v}\underline{x}_{lm}(t_k) = g_{w\to v}\left({}^{w}\underline{x}_{v0}(t_k) + {}^{w}\underline{v}_{v}(t_k), {}^{w}\underline{x}_{lm}(t_k)\right) \tag{13} $$

$$ {}^{m}\underline{y}_{lm}(t_k) = g_{v\to m}\left({}^{v}\underline{x}_{m0}(t_k), {}^{v}\underline{x}_{lm}(t_k)\right) + {}^{m}\underline{v}_{m}(t_k) \tag{14} $$

The position vector ${}^{w}\underline{x}_{v0}(t_k)$ contained in function $g_{w\to v}$ corresponds to the state space vector of the moving vehicle and can be substituted by ${}^{w}\underline{x}_{ctrv/v}(t_k)$. In order to simplify it is written in the further equations as ${}^{w}\underline{x}_{v}(t_k)$. The ${}^{w}\underline{v}_{v}(t_k)$ signal describes the disturbances of the vehicle state space vector, i.e. the uncertainty of the actual estimation.

The combination of the two steps (13) and (14) leads to

$$ {}^{m}\underline{y}_{lm}(t_k) = g_{v\to m}\left({}^{v}\underline{x}_{m0}(t_k), g_{w\to v}\left({}^{w}\underline{x}_{v0}(t_k) + {}^{w}\underline{v}_{v}(t_k), {}^{w}\underline{x}_{lm}(t_k)\right)\right) + {}^{m}\underline{v}_{m}(t_k). \quad (15) $$

Taking into account that the disturbances ${}^{w}\underline{v}_{lm}(t_k)$, ${}^{w}\underline{v}_{v}(t_k)$ and ${}^{v}\underline{v}_{m}(t_k)$ are mean value free

$$ E\left\{{}^{w}\underline{v}_{lm}(t_k)\right\} = 0\,,\; E\left\{{}^{w}\underline{v}_{v}(t_k)\right\} = 0\,,\; E\left\{{}^{v}\underline{v}_{m}(t_k)\right\} = 0 \quad (16) $$

and the according covariance matrices are defined by

$$ E\left\{{}^{w}\underline{v}_{lm}(t_k)\cdot{}^{w}\underline{v}_{lm}(t_k)^{T}\right\} = {}^{w}P_{lm}\,, \quad (17) $$

$$ E\left\{{}^{w}\underline{v}_{v}(t_k)\cdot{}^{w}\underline{v}_{v}(t_k)^{T}\right\} = {}^{w}P_{v}\,, \quad (18) $$

$$ E\left\{{}^{m}\underline{v}_{m}(t_k)\cdot{}^{m}\underline{v}_{m}(t_k)^{T}\right\} = {}^{m}R_{m}\,, \quad (19) $$

we end up with

$$ {}^{m}\hat{\underline{y}}_{lm}(t_k) = g_{v\to m}\left({}^{v}\underline{x}_{m0}(t_k), g_{w\to v}\left({}^{w}\underline{x}_{v0}(t_k), {}^{w}\underline{x}_{lmo}(t_k)\right)\right) \quad (20) $$

for the expectation value of the complete measurement transformation for a specific landmark *lm*.

For the corresponding transformation of the uncertainties we use the Jacobi matrices of the both non-linear functions

$$ g_{w\to v}(t_k) \Rightarrow C_{w\to v}(t_k)\,, \quad (21) $$

$$ g_{v\to m}(t_k) \Rightarrow C_{v\to m}(t_k) \quad (22) $$

and end up with

$$ {}^{m}U_{lm} = E\left\{{}^{m}\underline{y}_{lm}(t_k)\cdot{}^{m}\underline{y}_{lm}(t_k)^{T}\right\} \quad (23) $$

$$ {}^{m}U_{lm} = C_{v\to m}\left(C_{w\to v}\left({}^{w}P_{v} + {}^{w}P_{lm}\right)C_{w\to v}^{T}\right)C_{v\to m}^{T} + {}^{m}R_{m}\,. \quad (24) $$

The transformation $g_{w\to v}(t_k)$ is the same for both expected types of landmarks (and sensors). It contains the spatial transformation step

$$ \begin{bmatrix} {}^{v}x_{lm}(t_k) \\ {}^{v}y_{lm}(t_k) \end{bmatrix} = R\left({}^{w}\gamma_{v0}(t_k)\right)^{-1}\left(\begin{bmatrix} {}^{w}x_{lm}(t_k) \\ {}^{w}y_{lm}(t_k) \end{bmatrix} - \begin{bmatrix} {}^{w}x_{v0}(t_k) \\ {}^{w}y_{v0}(t_k) \end{bmatrix}\right) \quad (25) $$

and is the basis for the calculation of $C_{w\to v}(t_k)$.

4.1 Point-Style Landmarks

Point-style landmarks in the presented system are detected with a laser scanner as it is visualized in figure 8 [13]. The transformation step $g_{v\to m}(t_k)$ is defined for the laser by the equations [8]

$$ \begin{bmatrix} {}^{l}r_{lm}(t_k) \\ {}^{l}\phi_{lm}(t_k) \end{bmatrix} = \begin{bmatrix} \sqrt{{}^{v}x_{lm}(t_k)^2 + {}^{v}y_{lm}(t_k)^2} \\ \arctan\left[\dfrac{{}^{v}y_{lm}(t_k)}{{}^{v}x_{lm}(t_k)}\right] \end{bmatrix} + \begin{bmatrix} v_r(t_k) \\ v_\phi(t_k) \end{bmatrix} \quad (26) $$

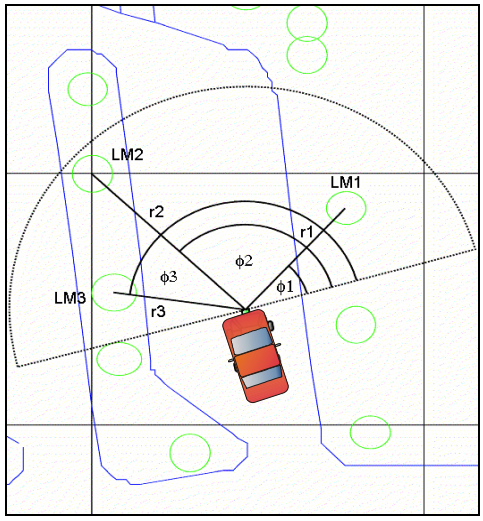

Fig. 8. Sensor vehicle measuring point-style landmarks with a laser scanner.

4.2 Line-Style Landmarks

The road border or parts of it are detected as line style landmarks in a video camera image [14]. On the basis of the map special measurement lines are created that allow the search along for the position of the border (see figure 9). To perform the search, these search lines are transformed into the image (figure 10).

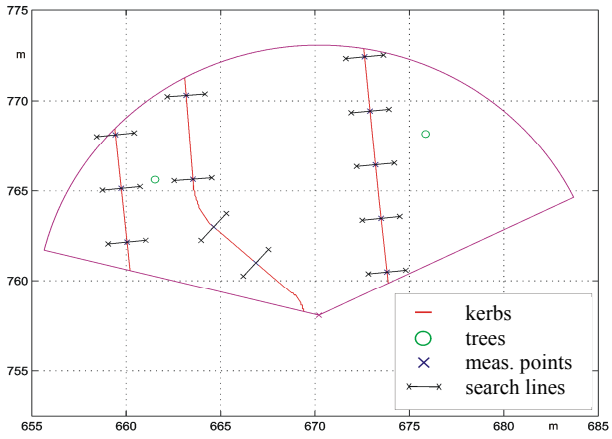

Fig. 9. Sensor vehicles field of view for detecting line-style landmarks with a CCD camera.

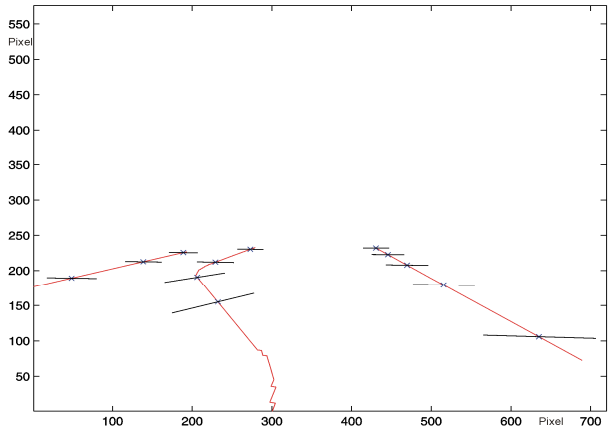

Fig. 10. Camera view of line-style landmarks.

In this way, line-style landmarks are detected by using line points as a representation of a line. To take the line characteristics into account, the uncertainty of the measured points is constructed in that way that the point possesses only a high certainty perpendicular to the line and no certainty parallel to the line (in reality a large uncertainty is used, see figure 11).
The transformation step $g_{v\to m}(t_k)$ for the camera is based on the 2D to 2D calibration parameters a_{lk} of the camera.

$$\begin{bmatrix} {}^{i}x_{lm}(t_k) \\ {}^{i}y_{lm}(t_k) \end{bmatrix} = \begin{bmatrix} \dfrac{a_{11}\,{}^{v}x_{lm} + a_{12}\,{}^{v}y_{lm} + a_{13}}{a_{31}\,{}^{v}x_{lm} + a_{32}\,{}^{v}y_{lm} + a_{33}} \\ \dfrac{a_{21}\,{}^{v}x_{lm} + a_{22}\,{}^{v}y_{lm} + a_{23}}{a_{31}\,{}^{v}x_{lm} + a_{32}\,{}^{v}y_{lm} + a_{33}} \end{bmatrix} + \begin{bmatrix} v_i(t_k) \\ v_j(t_k) \end{bmatrix} \quad (27)$$

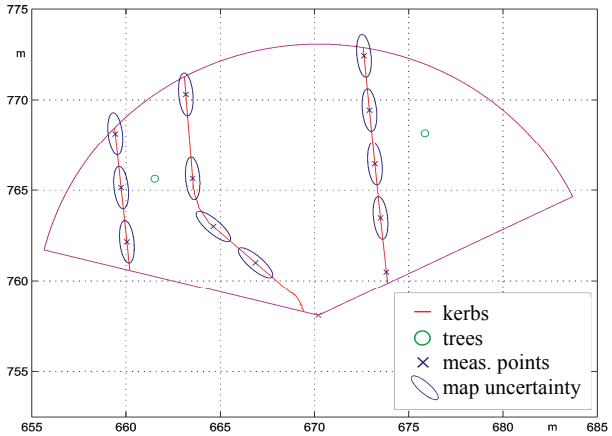

Fig. 11. Illustration of the map uncertainties of line-style landmarks.

5 Conclusions

The summarizing results, including the positioning component based on the two types of landmarks are shown in table 7. The good values of errors reached in section 3 could again be improved by using the landmarks. The mean square error reaches a better result for the point-style landmarks than for the line-style landmarks. The obvious reason for that is that the unique map uncertainty is additionally enlarged in the line direction.

Table 7: Performance of the position estimation system using landmarks.

Sensor combination	mean square error	maximum square error
only GPS	0.903 m (100.0 %)	2.913 m (100.0 %)
GPS, compass, long. velocity, angular velocity	0.278 m (30.1 %)	0.479 m (16.4 %)
camera LMs, GPS, compass, long. velocity, angular velocity	0.220 m (24.8 %)	0.370 m (12.8 %)
laser LMs, GPS, compass, long. velocity, angular velocity	0.070 m (7.7 %)	0.320 m (11.1 %)

The values reached for the maximum error seem to give hope for further work including landmark localization components. As the error values vary over time and are clearly dependent on the availability of landmarks, the combination of landmarks with different types in one system seems to be the best solution to combine spatial availability with the level of certainty provided by them.

Acknowledgements

For the active collaboration in the field of localization and simulation we thank the former and actual students of CUT at Communications Engineering laboratories Hendrik Neuber, Eric Richter, Daniel Seifert and Roman Thein.

References

[1] Y. Bar-Shalom, T. E. Fortmann. *Tracking and Data Association.* Academic Press, San Diego, 1988.

[2] Y. Bar-Shalom, X. Li, *Estimation and Tracking: Principles, Techniques, and Software.* Artech House, Delharn, MA, 1993.

[3] Norbert Haala, Jan Böhm. *A multi-sensor system for positioning in urban environments*. ISPRS Journal of Photogrammetry & Remote Sensing 58, 2003, 31–42, Elsevier 2003.

[4] X. R. Li, V. Jilkov. *Mathematical Models for Maneuvering Target Tracking: A Survey.* Third ONR/GTRI Workshop on Target Tracking and Sensor Fusion, Georgia Tech Research Institute, Cobb County Research Facility, Atlanta, Georgia, May 17-18, 2000.

[5] Ullrich Scheunert. *Fuzzy-Mengen-Verknüpfung und Fuzzy-Arithmetik zur Sensor-Daten-Fusion.*

Technische Universität Chemnitz, Dissertation, Fortschrittberichte VDI, Reihe 8, Nr. 941. VDI-Verlag GmbH Düsseldorf, 2002.

[6] Ullrich Scheunert, Heiko Cramer, Aris Polychronopoulos, Angelos Amditis, Gerd Wanielik, P. Claudio Antonello. *Multi sensor data fusion for object detection: challenges and benefit.* ATA-Conference ADAS, Siena, Italy, 2002.

[7] Ullrich Scheunert, Heiko Cramer, Gerd Wanielik. *Multi-Sensor-Daten-Fusion zur präzisen Lokalisierung von Fahrzeugen in Straßenumgebungen.* POSNAV, 2003, Deutsche Gesellschaft für Ortung und Navigation e.V., Tagungsband, Dresden, 18.-19. März 2003.

[8] Heiko Cramer, Ullrich Scheunert, Gerd Wanielik. *Multi Sensor Fusion for object detection using generalized feature models.* In Proceedings of the sixth Int. conference on Information Fusion, ISIF, pages 2-10, 2003.

[9] L. Simeonova, T. Semerdjiev. *Specific Features of IMM Tracking Filter Design.* INFORMATION & SECURITY. An international Journal, 9, 2002,154-165.

[10] E. Waltz, J. Llinas. *Multisensor Data Fusion.* (Art. H. adar/Electronic Warfare Library). Artech House Publishers, 1990.

[11] K. Brammer, G. Siffling. *Kalman Bucy Filter: Deterministische Beobachtung und stochastische Filterung.* R. Oldenburg,Muenchen, Wien, 1994.

[12] O. Loffeld. *Estimationstheorie II: Anwendungen - Kalman-Filter.* R. Oldenburg Verlag, Muenchen, Wien, 1990.

[13] Hendrik Neuber. *Lokalisierung von Fahrzeugen in Straßenszenen unter Verwendung von hochgenauen GIS-Karten und der Vermessung von Landmarken mit einem Laserscanner*. Diploma Thesis, Chemnitz University of Technology, 2002.

[14] Roman Thein. *Lokalisierung von Fahrzeugen in Straßenszenen unter Verwendung von hochgenauen GIS-Karten und der Vermessung von linienhaften Landmarken in Videobildern*. Diploma Thesis, Chemnitz University of Technology, 2002.